

Studying the Properties of Accretion Disks and Coronae in Black Hole X-ray Binaries with Monte-Carlo Simulations

Yangsen Yao^{1,2,3}, S. Nan Zhang^{1,2}, Xiaoling Zhang^{1,2}, Yuxin Feng^{1,2}, Craig R. Robinson⁴

ABSTRACT

Understanding the properties of the hot corona is important for studying the accretion disks in black hole X-ray binary systems. Using the Monte-Carlo technique to simulate the inverse Compton scattering between photons emitted from the cold disk and electrons in the hot corona, we have produced four table models in the *XSPEC* format for different configurations of corona system, i.e., the thermal or power-law electron energy distribution in a spherical or disk-like corona. All parameters in our table models are physical properties of the corona system and can be derived from fitting data directly. Applying the models to broad-band spectra of the black hole candidate XTE J2012+381 observed with BeppoSAX, we estimate the size of the corona and the inner disk radius. According to the fitting results with our table models, in XTE J2012+381 system, the size of the corona with a spherical geometry is several tens of gravitational radius. Under these models, the substantial disk radius increases from hard-state to soft-state is not found and the inner disk radius is nearly a constant.

Subject headings: accretion, accretion disks — black hole physics — X-rays: binaries — X-rays: individual (XTE J2012+381)

1. Introduction

A black hole X-ray binary (BHXB) system consists of a compact object ($> 3M_{\odot}$) and its companion star. Material can be transferred from the companion to the compact object

¹Physics Department, University of Alabama in Huntsville, Huntsville, AL 35899; yaoy@email.uah.edu, zhangsn@email.uah.edu, xizhang@jet.uah.edu, fengyx@jet.uah.edu

²National Space Science and Technology Center, 320 Sparkman DR., SD50, Huntsville, AL 35805

³Present address: Department of Astronomy, University of Massachusetts, Amherst, MA 01003; yaoy@astro.umass.edu

⁴Division of Information Systems, National Science Foundation, 4201 Wilson Blvd, Arlington, VA 22230; crobinso@nsf.gov

either through Roche lobe overflow or via a stellar wind (accretion process). Because the accreting matter must lose its angular momentum before it can be “swallowed” by the compact object, an accretion disk is usually formed and the gravitational potential energy of the accreting matter is released through radiation. The X-ray spectrum of a black hole X-ray binary system usually can be well fit with two-component model: a black-body-like component and a power-law-like component (Tanaka & Lewin 1995). The black-body-like component turns off above 20 keV and is believed to be emitted from the accretion disk. The power-law-like component can extend up to 200 keV, which suggests that a high temperature electron cloud (corona) exists above the accretion disk and the inverse Compton scattering between the disk photons and electrons in the corona is the main mechanism to produce this component.

In the X-ray astronomy community, the multi-color disk model (MCD) (*diskbb* in *XSPEC*, Mitsuda et al. 1984; Makishima et al. 1986) plus a power-law model has been employed traditionally to fit the energy spectra of the black hole X-ray binary systems, then the parameters of the MCD model are used to infer the physical parameters of the accretion system. However, this model is over-simplified in the following two aspects.

First, the assumption that the power-law component extends straight to the low-energy limit of the spectrum is unreasonable, since the power-law component is believed to be produced by inverse Compton scattering. The most natural source of the seed photons is the thermal radiation from the accretion disk; they are of the same origin as the black-body-like component. Therefore a low-energy cutoff must be present in the power-law component, since the seed photon distribution has a peak energy below which there are only a small amount of seed photons. Neglecting this low-energy cutoff by applying a simple power-law spectrum model would under-estimate the flux in the black-body-like component.

Second, it has been a rather standard approach by many (including the some authors of this paper) in the field to take the black-body-like flux derived from the spectral model fitting as the true flux of the accretion disk and infer the inner disk radius from it. This ignores the radiative transfer process in the production of the power-law component. Since the power-law component is likely produced by scattering the soft photons in the original black-body-like component of the accretion disk, each photon in the power-law component comes at the expense of a lost photon in the black-body-like component, even if no absorption occurs in the Comptonization process. Therefore certain corrections are needed to infer the original flux of the black-body-like component, otherwise the real flux would be under-estimated, as realized by some authors (e.g., Kubota, Makishima & Ebisawa 2001), which might be the reason that the inner disk radius varies significantly when an accretion system transits from its hard state to its soft state or vice versa, like in XTE J1550-564 (Sobczak et al. 1999a),

GRO J1655-40 (Sobczak et al. 1999b), XTE J2012+381 (Campana et al. 2002), etc..

In order to estimate the true flux of the accretion disk and then to estimate the inner disk radius, one needs to establish an intrinsic relation between the soft (low energy) photons and hard (high energy) photons, then do a radiative transfer correction to recover the original flux of the accretion disk, which inevitably needs to calculate the Comptonized spectra. The Comptonized spectra have been computed by many authors using different approaches.

One of the analytical approaches was carried out by assuming an optically thick non-relativistic plasma and then solving the Kompaneets equation either numerically or analytically (e.g., Sunyaev & Titarchuk 1980; Payne 1980). This approach was improved later on by Titarchuk (1994, T94 hereafter) and Titarchuk & Lyubarskij (1995, TL95 hereafter) and could be applied to both non-relativistic and relativistic plasma, which was further verified by Hua & Titarchuk (1995, hereafter HT95) by using different analytical approximations and Monte-Carlo simulations. In their paper, HT95 pointed out that there is an applicability region of the analytical generalized Comptonization models of T94 and TL95 in the $\beta - kT_e$ parameter plane in which these models agree with the Monte-Carlo simulation fairly good (see Fig. 7 of HT95).

Another approach is to calculate radiative transfer by using Monte-Carlo technique (e.g., Corman 1970; Loh & Garmire 1971; Pozdnyakov, Sobol' & Sunyaev 1977; Fenimore et al. 1982; etc.). This method has been described in detail by Pozdnyakov, Sobol' & Sunyaev (1977, PSS77 hereafter) and has been significantly improved by Gorecki & Wilczewski (1984) by removing the inaccurate assumption made by PSS77 that the probability for a collision between a photon and an electron is independent of the electron energy and the scattering angle. Those works mentioned above take the Compton scattering process as main process when computing the Comptonized spectra from hot plasmas, some other authors also take into account other important physic process like bremsstrahlung, pair production (e.g., Skibo et al. 1995) and disk-reflection (e.g., Haardt & Maraschi 1991).

Recently, Poutanen & Svensson (1996, hereafter PS96), by taking into account almost all important physical processes in the hot plasmas and by solving the radiative transfer equation iteratively for each scattering, built a new model to describe the emergent spectra from the plasmas, which has been successfully tested with Monte-Carlo simulations (Stern et al. 1995).

However, all these works (using both analytic and Monte-Carlo approaches) emphasize on computing the accurate emergent photon spectra and none of them can be used directly to address the problem in studying BHXB systems we mentioned above, i.e. recovering the original flux of the accretion disk in the spectral fitting self-consistently and then calculating

the true inner disk radius.

In this paper, we only consider Compton scattering process in the hot plasma (corona) and use the Monte-Carlo technique to compute the emergent photon spectra from the corona; four table models (as the standard model in *XSPEC* package) have been built based on our simulated spectra. Using these table models to fit the data on XTE J2012+381 with BeppoSAX, we can estimate directly the size and optical depth of the corona, the inclination angle and the real flux of the accretion disk (and thus the inner disk radius).

This paper is organized as following. In section 2 of this paper, our Monte-Carlo simulation is introduced, and in section 3 the results of applying our table models to the source XTE J2012+381 is reported. Finally summary and discussion are presented in section 4.

2. Monte-Carlo simulations and table models

2.1. Assumptions

In our simulations, we assume that the accretion disk is an optically thick Keplerian disk (Mitsuda et al. 1984), and during the accretion process, the accretion rate (\dot{m}) is constant and the gravitational potential energy loss of the accreting material is radiated away in black-body radiation locally. Therefore the temperature radial profile is $T(r) \sim r^{-3/4}$, as in the MCD model (Mitsuda et al. 1984; Makishima et al. 1986). We also assume that the corona above the accretion disk may take either spherical or disk geometry, the electron density distribution in the corona is uniform, and the electron energy distribution in the corona may take either thermal form or non-thermal form (we simply take the power-law for non-thermal distribution), as done in previous works (Hua & Titarchuk 1995; Titarchuk 1994; Poutanen & Svensson 1996); the disk reflection is ignored, and the energy loss of the corona during the Compton scattering process is negligible.

2.2. Simulations

We sample photons for a given combination of the above parameters of a system, e.g., the temperature of the inner boundary of the accretion disk, the size of the corona (for a spherical corona system, the size is defined as the value of its radius; for a disk-like corona system, it is defined as the vertical height), the power-law index of the electron energy distribution or the temperature of the electron in the corona, the optical depth of the corona (defined as $\tau = \int n_e \sigma_T dl$, where n_e is electron density, σ_T is Thompson scattering cross

section and the integral is along the radial direction in the spherical corona case and along the vertical direction in disk-like corona case), etc.. Since for any ring on the accretion disk, the radiation is taken as a black body locally, the number of photons released from a ring on the accretion disk is,

$$\begin{aligned} dN_{ph} &= a^* T^3 2\pi r dr \\ &\propto r^{-5/4} dr, \end{aligned} \quad (1)$$

where

$$a^* = \frac{2\pi}{c^2} \left(\frac{k}{h}\right)^3 \int_0^\infty \frac{x^2 dx}{e^x - 1},$$

c is the speed of light, k is Boltzmann's constant and h is Planck's constant. The photon energies follow blackbody distribution with temperature $T(r)$ and the initial direction of a photon is sampled uniformly in 4π solid angles. In a spherical corona system, the corona covers a portion of the disk, then a photon emitted from the disk in this kind of system, depending upon the emitting location and the initial direction, may or may not enter the corona. In disk-like corona systems, the corona covers the whole disk but its vertical size may vary, then a photon emitted from the disk always enters the corona first.

After a photon enters the hot corona, the probability (ρ) to interact with an electron is related to its free-path distance,

$$d\rho \propto e^{-\tau_l} d\tau_l, \quad (2)$$

and

$$d\tau_l = \sigma_{K-N} n_e dl, \quad (3)$$

where τ_l is the optical depth of the free-path distance along the moving direction, σ_{K-N} is Klein-Nishina cross section (Berestetski, Lifshitz, & Pitaevski 1972),

$$\sigma_{K-N}(x) = 2\pi r_0^2 \frac{1}{x} \left[\left(1 - \frac{4}{x} - \frac{8}{x}\right) \ln(1+x) + \frac{1}{2} + \frac{8}{x} - \frac{1}{2(1+x)^2} \right], \quad (4)$$

and

$$x = \frac{2h\nu}{m_e c^2} \gamma (1 - \bar{v} \cdot \bar{\Omega}/c),$$

$h\nu$, $\bar{\Omega}$ are the energy and the direction of the incident photon in the laboratory frame, \bar{v} is the electron velocity, r_0 is the classical electron radius ($r_0 = e^2/mc^2$) and $m_e c^2$ is the electron rest mass energy. It is obvious that the σ_{K-N} depends on the incident photon energy, electron energy and their moving directions. In order to determine the photon free-path distance l in equation 3, we need to calculate σ_{K-N} , therefore we need to know the electron energy (E_e) along a sampled direction, which usually is a function of the photon's free-path distance, i.e., the dependency relation for equation 3 is like, $l \rightarrow \sigma_{K-N} \rightarrow E_e \rightarrow l$. To simplify this problem, we assume that the energy distribution in the corona is uniform,

then the dependency between E_e and l is no longer needed. However, the sampling of the electron information is not trivial, because it is related to the input photon information and the total Compton cross section $\sigma_{K-N}(x)$,

$$\rho(\bar{v}) \propto N(\bar{v})(1 - \bar{v} \cdot \bar{\Omega}/c)\sigma_{K-N}(x), \quad (5)$$

where, $N(\bar{v})$ is electron distribution which is further assumed to be isotropic and follows a thermal form $dN_e \propto e^{-E_e/kT} \sqrt{E_e} dE_e$ or a power-law form $dN_e \propto \gamma^{-\Gamma_e} d\gamma$, T is the temperature of the corona, γ is the Lorentz factor (indicating the total energy of the electron), Γ_e is the power-law index of electron's energy distribution.

The equation 5 is a two-dimensional probability distribution, which is rather complicated to obtain and has been addressed in the previous works (Sobol' 1974; Górecki & Wilczewski 1984). In our simulation, we adopt the simple algorithm developed by Hua (1997) to sample the electron energy E_e and its moving direction $\bar{\Omega}_e$. Therefore σ_{K-N} can be calculated (the photon energy and moving direction are known) and the photon's free-path distance can be derived using equation 3.

After each interaction, the scattered photon direction can be sampled by using the differential cross section (Akhiezer & Berestetski 1965), which is related to electron velocity (\bar{v}) and the incident photon energy and direction, and the scattered photon energy. However, in the electron's rest frame, the formula is relatively simple (Klein & Nishina 1929),

$$\frac{d\sigma}{d\Omega} = \frac{1}{2} r_0^2 \left(\frac{h\nu}{h\nu_i} \right) \left(\frac{h\nu}{h\nu_i} + \frac{h\nu_i}{h\nu} - \sin^2 \theta \right), \quad (6)$$

where, θ is the scattering angle, $h\nu_i$ and $h\nu$ are incident and scattered photon energy in the electron's rest frame and related to each other by

$$h\nu = \frac{h\nu_i}{1 + \frac{h\nu_i}{m_e c^2} (1 - \cos \theta)}. \quad (7)$$

Therefore, after sampling the electron energy and direction, we transform the incident photon information to the electron's rest frame, and replace the scattered photon energy ($h\nu$) in equation 6 with equation 7, then the scattered photon direction can be sampled. In the end, the scattered photon energy can be calculated easily.

After zero or more scattering with electrons, an initially incident photon will escape and the escaped photons will form a spectrum as a function of the inclination angle. In our simulation process, we ignore the disk reflection mechanism, i.e., a photon is assumed to be absorbed by the accretion disk when it collides with the accretion disk.

It is worth noting that unlike the method described by Górecki & Wilczewski (1984), we trace each single photon from its emitted location until it escapes from the disk-corona

system, then record it as a single event, i.e., each recorded photon has exactly the same statistical weight as others. In this manner, we sacrifice the simulation efficiency to avoid calculating the escape probability and the scattering probability distribution in each scattering. Therefore our Monte-Carlo code has been sufficiently simplified and its efficiency obviously depends on the configuration of the disk-corona system (especially on the optical depth of the corona); the total computation time is also tolerable (e.g., it takes 5 minutes to produce 500,000 events for a spherical corona with optical depth around unit when running on Intel Xeon CPU 1.50GHz).

2.3. Simulation results

Our simulation results can be summarized as following. In Fig 1 to Fig 6, the input parameters are listed in the plot for the corresponding spectrum.

1) When the electron energy distribution in the corona has a thermal form, the high energy profile of the spectrum is determined by the so called y -parameter (Longair 1992) (Fig 1), which is defined as

$$y = \frac{4kT_e}{m_e c^2} \max(\tau, \tau^2), \quad (8)$$

where T_e is electron thermal temperature, m_e is electron rest mass and τ is the optical depth of the corona. For the coronae with the same optical depth, the higher the electron temperature is, the harder the spectrum will be (Fig 1.a, 1.c). This is because the net energy change of the photon in a Compton collision is (see e.g., Longair 1992)

$$\frac{\Delta E}{E_0} = \frac{-E_0 + 4kT_e}{m_e c^2}, \quad (9)$$

which implies that a photon will gain more energy in each collision in a hotter corona, and also indicates that the photon spectrum will turn off at the energy around $4kT_e$. With the same electron temperature, the output spectrum will be harder in a denser corona (Fig 1.b, 1.d), because on average, a photon will suffer more scattering by the electrons in the corona and eventually gain more energy.

2) When the electron energy distribution has a power-law form in the corona, the high energy part of the spectrum also has a power-law-like tail and the photon index is mainly determined by the power-law index of the electron (Fig 2). With the same optical depth of the corona, the output spectrum will be harder if the electron power-law index is smaller (harder) in the corona (Fig 2.a). With the same electron power-law index, the larger the optical depth of the corona is, the more soft photons will be up-scattered to high energy

band but the photon indices are similar (Fig 2.b). This is because, when the electrons are relativistic, the photon index of the spectrum is related to the electron index through

$$\Gamma = \frac{\Gamma_e + 1}{2}, \quad (10)$$

where Γ is the photon spectral index (Rybichi & Lightman 1979).

3) When the electron energy distribution in the corona has different forms, the spectral shape in the high energy band is different; electron energy distribution with power-law form produces a power-law-like hard tail without obvious turn-off in the spectrum, and thermal electron energy distribution produces a spectrum with obvious turn-off point at the energy around 4 times of the electron thermal temperature (Fig 3). The electron energy distribution in the corona can be described by a unique parameter, kT or Γ_e , for a thermal form or a power-law form respectively, and each of these two parameters is one of the key parameters to determine the shape of the spectra.

4) The temperature of the inner accretion disk boundary determines the turning point in the soft band of the spectrum (Fig 4). According to the temperature radial profile we assumed, the inner disk boundary has the highest temperature along the disk. For the photon flux distribution of a black body, the maximum is at the energy around 1.6 times of its temperature. Therefore, the seed photon spectrum should have a turning point around 1.6 times the temperature of the inner disk boundary.

5) For a system with a spherical corona, the low energy band of the output spectrum is related to the size of the corona (Fig 5.a and 5.b), whereas for a system with the disk-like corona, the output spectrum has no such kind of relation (Fig 5.c and 5.d); a larger spherical corona will cover the farther outer part of the accretion disk, then when other parameters (especially the optical depth) are equal, the photons with lower energy will be scattered to the high energy band. However, in a system with the disk-like corona, the corona always covers the whole disk and the vertical height does not affect the shape of the output spectrum, i.e., the output spectra with different height of the corona are identical as long as the other parameters (especially the optical depth) are equal.

6) For a spherical corona, the flux of the soft component of the spectrum at different inclination angle differs by a cosine factor and the hard component is almost isotropic except for at very high inclination region (Fig 6.a and 6.b), whereas for a disk-like corona, both the soft component and the hard component are related to the inclination angle by a cosine-like factor (Fig 6.c and 6.d). In a spherical corona system, the optical depth of the corona has nearly the same value when viewed from different inclination angles (strictly speaking, the optical depth is slightly different for different inclination angle if considering the seed photon distribution along the accretion disk. This difference is obvious when the inclination angle

of the disk is high.). The flux of the soft component is proportional to the projected area of the disk perpendicular to the line of sight. Since the optical depths for different inclination angles are the same and the electron’s moving direction in the corona is isotropic, the flux of the hard component is almost isotropic. Whereas in a disk-like corona system, in addition to the effective area due to the projection, the optical depth of the corona also depends on the view angle; a smaller angle corresponds to a smaller optical depth, thus more disk photons can escape directly.

2.4. Comparison with T94 and PS96

We compare the angle-averaged Comptonized spectra calculated by our simulation with those from the analytic formulae for thermal Comptonization from the papers by T94 and those obtained from using the iterative scattering method by PS96 (Fig 7). In our simulation and the calculation by PS96, the incident photons are from the center of a spherical corona and follow the Planck’s formula, and in the computation by T94, the incident photons were assumed to follow the Wien form. The other input parameters are listed in Fig 7. The two different cases in the plot correspond to two different regimes specified by HT95 (please refer to Fig. 7 of HT95). For the comparison, it can be seen that our results are closer to those of T94 than to those of PS96. The difference between our results and those of PS96, we believe, is due to the consideration of the energy balancing in PS96, in which the Compton cooling could be significant when the corona becomes more opaque to Compton scattering. Our work, as in T94, assumes that a steady state of the electron’s temperature distribution has already been achieved, regardless of the detailed physical process in achieving this equilibrium condition.

2.5. Table models

Using the simulated spectra, we have built four table models¹ for spherical and disk-like corona with thermal and power-law electron energy distributions respectively. The table models consist of the following parameters: temperature of the inner boundary of the accretion disk (T_{in}), thermal electron temperature (kT , for thermal electron energy distribution) or the electron power-law index (Γ_e , for power electron energy distribution), radial size of the spherical corona; $Size$, in unit of $R_g = GM/c^2$, where M is the black hole mass), optical depth of the corona (τ), inclination angle of the accretion disk (θ), and

¹ftp://legacy.gsfc.nasa.gov/caldb/docs/memos/ogip_92_009/ogip_92_009.ps

normalization parameter (K_{norm}) which is added by the *XSPEC* automatically and related to the disk radius by the formula $K_{norm} = ((R_{in}/km)/(D/10kpc))^2$, where D is the distance of the source (for detail, please see Appendix). Since for the disk-like corona, the spectra with different size of the coronae are identical (please refer to Fig. 5.(c) and (d)), the *Size* parameter does not exist in the table models for the disk-like coronae.

3. Application to XTE J2012+381

The X-ray transient XTE J2012+381 was discovered with the Rossi X-ray Timing Explorer All Sky Monitor (RXTE-ASM) on May 24, 1998 (Remillard et al. 1998). Its spectra observed with ASCA consist of a soft thermal component (with temperature around 0.8 keV) and a hard power-law tail (with photon index around 3) (White et al. 1998), which is considered to be indicative of a spectrum of black hole candidates (Lewin, Van Paradijs & Van Den Heuvel 1995). Five observations were carried out with BeppoSAX from 1998 May 28 to 1998 July 8 (Fig 8.a). The spectra with the narrow field instruments LECS (Parmar et al. 1997) and MECS (Boella et al. 1997) were extracted with a radius of 8' centered on the source position. The background subtractions for these two instruments were obtained using blank sky observations. HPGSPC (Manzo et al. 1997) and PDS (Frontera et al. 1997) data were extracted using SAXDAS (hpproducts V3.0.0) and XAS respectively. All our spectral analyses were carried out in the energy range suggested by the BeppoSAX cookbook²: 0.12-4 keV for the LECS, 1.65-10.5 keV for MECS, 8-20 keV for the HPGSPC, 15-220 keV for PDS, and a 2% systematic errors were added during our data analysis to account for the uncertainties in the calibrations. The public software package *XSPEC* 11.0.1 was employed in our analysis.

As usual, MCD (Mitsuda et al. 1984; Makishima et al. 1986) plus a power-law and a Gaussian line model was used first to fit the data, which can describe the observations very well (χ^2 is 177 with 144 DOF, Fig 8(b)). The best fit parameters are similar to the previous reported by Campana et al. (2002).

Our four table models were then applied to the data, which, together with a broad Gaussian line, all provide reasonably good fits to the entire BeppoSAX observations (Fig 8(c)-8(f)) and the best fit parameters are reported in Table 1. Since we mainly focus our efforts on the continuum, the line parameters are not reported in Table 1. According to our simulation results, the output spectrum is insensitive to the corona size in a disk-like geometrical system, so we fix the size of the corona to 20 times of gravitational radii when analyzing data with

²<http://heasarc.gsfc.nasa.gov/docs/sax/abc/saxabc/saxabc.html>

our table models for the disk-like corona systems.

According to the fitting results, the column density nearly remains constant with a mean central value $1.33 \times 10^{22} \text{ cm}^{-2}$, and the temperature at the inner accretion disk is around 0.72 keV, which agree with the previous report (Campana et al. 2002). For a power-law electron energy distribution model, the electron power-law index (Γ_e in model-A and model-B in Table 1) increases, indicating the spectra become softer and softer during the BeppoSAX observations except for the last observation. The upper limit of the electron power-law index in the last two observation is even beyond the parameter range of the table models (the parameter range in our table models is 2 to 6 so far). This is because the spectrum is very soft, resulting in a poor statistical quality in the high energy band, thus a poor constraint on the electron power-law index. For the thermal electron energy distribution model, the electron temperature (kT in model-C and model-D in Table 1) in the corona decreases during the BeppoSAX observations. In the first two observations, the upper limit of the electron temperature in the corona is beyond the parameter range (current range is 5 keV to 200 keV) in our table models. The reason is that in the first two observations, the spectra are very hard, and there is no obviously cut-off within the sensitive energy ranges of the instruments. In the last three observations, the spectra are relatively soft and the temperature can be constrained well. If the system has a spherical corona, the size of the corona may vary from several tens to one hundred times of the gravitational radii and each has a very large range of uncertainty, which is due to the insensitivity of the instrument below 0.1 keV. The small size of the corona also indicates that, if the system has a spherical corona, the hard photons are mainly generated within a very small region near the central compact object.

Determining the optical depth of the corona is coupled to the determination of the inclination angle of the accretion disk (see discussion below), and the variation of the inferred inclination angle causes some variations on the normalization of our table models, which is related to the inner radius of the accretion disk. According to the previous report by Campana et al. (2002), the inner disk radius increases “sharply” from 33 km in the first observation (in which the power-law component is relatively strong) to 38 km in the rest four observations (in which the power-law component is relatively weak). We believe that the apparent changes of the disk radius are due to disregarding the origin of the hard component as we mentioned in the introduction. In order to make a comparison of the results between ours and those by Campana et al. (2002), we normalize all disk radius to an inclination angle at zero degree (Fig 9). In order to study the evolution of the disk radius and reduce the uncertainties caused by the uncertainties of the inclination angle and the absorption (Hydrogen density), we fix the Hydrogen density to $1.33 \times 10^{22} \text{ cm}^{-2}$ and the inclination angle θ at 40 degrees, then re-analyze the data. The normalization parameter of our table

models are reported in the Table 1 and the normalized (at zero inclination angle) disk radius are also plotted in Fig 9. From the figure, it can be seen that the radius of the accretion disk inferred from our table models is almost a constant around 34 km.

4. Conclusion and discussion

According to our simulation results, the X-ray spectral shape in the high energy band is related to the y —parameter for a system with a thermal electron energy distribution in the corona and is related to the electron power-law index if the electron energy distribution follows a power-law form. For a system with a spherical corona, the spectral shape in the low energy band is related to the size of the corona, and the dependency of the flux of the soft component on the inclination angle follows a cosine function, whereas the flux of the hard component is nearly isotropic. For a system with a disk-like corona, the flux of both the soft and the hard components depend on the inclination angle by a cosine-like function.

Four table models have been built based on our simulation results and the physical parameters can be obtained directly when modelling the data with these table models. According to the fitting results with our table models, the electron energy distribution in the corona of XTE J2012+381 during the rising phase (the first observation) may either have a power-law form with index around 4 or have a Maxwellian form with thermal temperature around 200 keV or above. If the corona takes a spherical geometry in the system, the size of the corona may vary from less than 10 to 100 times of gravitational radii.

The reason that the size of the corona can be determined from the X-ray spectral fitting is that in our models the seed photons for the inverse Compton scattering come from the disk, on which the temperature is a function of the distance from the central black hole. The relatively small size of the corona indicates that most of the hard X-ray photons come from the region very close to the black hole. As we pointed out in section 2, the size of the corona is inferred from the spectral shape at the low energy band. Therefore, the future instruments with good response at the low energy band (less 0.1 keV) will help in reducing the uncertainties in determining the size of the corona.

Another interesting result is the determination of the disk inclination angle in spectral fitting with our table models. The reason that the inclination angle can be inferred is that the observed flux from the disk depends strongly upon the inclination angle (through a cosine factor), whereas the hard X-ray flux is almost isotropic, especially for the case of spherical corona. For the case of disk-like corona, the hard X-ray flux also depends upon the disk inclination angle. The inclination angle is always coupled with the optical depth of

the corona, which is also related to the ratio of the flux of the soft component to the flux of the power-law component. Thus, inferring the disk inclination angle by spectral fitting may have some ambiguities.

Determining the value of the inner disk radius is important in understanding the physics of the accretion disk and the black hole angular momentum (Zhang et al. 1997). The normalization parameter inferred with our table model, which is proportional to square of the inner disk radius, is nearly constant in the entire BeppoSAX observations, and the previously reported sharp increase of the disk radius from the hard state to the soft state did not happen according to the fitting results with our table models. This is because the corona, though optically thin in most cases, scatters some of the photons emitted from the disk and makes the observed soft component different significantly from the original disk emission. Using the simple *diskbb + powerlaw* model and without considering the origin of the power-law like component will certainly under-estimate the real flux of the blackbody-like component, especially when the source is in the hard state. The reason that we can estimate the real flux of the accretion disk is that the number of the photons emitted from the disk is known in our Monte-Carlo simulations.

In this study, we did not use the inferred inner disk radius to further derive the radius of the last marginally stable circular orbit and the black hole spin of the system. Please be noted that the gravitational potential assumed in this study is still Newtonian potential, which could be substantially different from the real potential in the vicinity of a black hole (Gierliński et al. 1999, 2001). Therefore in order to derive the radius of the last marginally stable circular orbit and the black hole spin, several effects need to be taken into account, which include the difference between the innermost radius and the peak temperature radius of the accretion disk, the color temperature change and flux change due to the general relativity (Cunningham 1975; Zhang, Cui, & Chen 1997). Fortunately, Zhang, Cui, & Chen (1997) tabulated these effects as different correction factors in their work and these factors have been proved to be reasonably accurate (Gierliński et al. 2001). In this work, we emphasize on introducing our Monte-Carlo simulation method and table models, and the applications of these models to some ultra-luminous X-ray sources (Wang et al. 2004) and to the two permanent X-ray sources LMC X-1 and LMC X-3 (Yao et al. 2004) have been performed and will be published soon.

Our table models, avoiding to use the two-isolated-component model then do the complicated radiative transfer correction to infer the real flux of the accretion disk, can treat the observed spectrum consistently and derive the physics parameters of the accretion system directly from the model-fit. However, when the spectral hardening effect needs to be considered, which is due to disk structure (Zhang et al. 2000; Nayakshin & Dove 2001) or

the Compton scattering process between the disk photon and the electron around the inner disk region (Shakura & Suniaev 1973; Shimura & Takahara 1995), or when the disk reflection component is important in the observed spectrum, a more complicated Monte-Carlo simulation is needed to infer the real flux of the accretion disk.

Modelling broad-band X-ray continuum spectra with physically consistent and accurate models provides a powerful tool in determining the properties of accretion disks and coronae in black hole X-ray binaries. However such studies require high quality and broad-band data, which may be provided by BeppoSAX, Chandra and XMM-Newton currently. Future data from Integral, Swift and especially the Constellation X-ray missions will provide significant breakthroughs in this field.

Unfortunately, in our table model, the normalization parameter is very sensitive to the inclination angle parameter, which, as mentioned before, is coupled together with the optical depth parameter. In order to reduce the uncertainties of the value of the normalization parameter in our table model and to infer the real flux of the accretion disk, an accurate inclination value is highly needed and the optical observations may give useful help on this issue.

Currently, we have not included non-uniform corona in our table models. The general relativistic effects and Doppler effects (Zhang, Zhang & Yao 2001) are not taken into account either. These will be our future work.

We thank the anonymous referee for critical, yet insightful comments on our manuscript, which made us to improve the paper substantially. Mr. Yongzhong Chen is acknowledged for his initial work on this project during his visit to UAH in 1999-2000. We want to give our special thanks to Dr. S. Campana for kindly giving us the data of XTE J2012+381 observed with BeppoSAX. We also thank Drs. Lev Titarchuk and Wei Cui for interesting discussions and Dr. Alan Harmon for useful comments. This work was supported in part by NASA Marshall Space Flight Center under contract NCC8-200 and by NASA Long Term Space Astrophysics Program under grants NAG5-7927 and NAG5-8523.

A. Normalization parameter in our table models

Starting from a multi-color disk black body, assuming the inner disk temperature is T_{in} and the inner disk radius is R_{in} , then the total number of photons released by the disk per unit time will be (by integrating Plank function from R_{in} to infinity),

$$ph = 8\pi a^* T_{in}^3 r_{in}^2 \quad (A1)$$

where, $a^* = \frac{2\pi}{c^2} \left(\frac{K}{h}\right)^3 \int_0^\infty \frac{x^2 dx}{e^x - 1}$ Thus, the observed photon flux at distance D with inclination angle θ will be,

$$\begin{aligned} F_{ph}(\theta)ds &= ph(\theta)d\Omega \\ &= 8\cos(\theta)a^*T_{in}^3r_{in}^2\frac{ds}{D^2} \\ &= 8\cos(\theta)a^*T_{in}^3\left(\frac{r_{in}}{D}\right)^2ds. \end{aligned} \quad (\text{A2})$$

If considering the double sides of the accretion disk, there should be another factor 2 in equation (A1) and (A2). However, in our calculation, we only consider one side and it is self-consistent within our table model.

In our simulation, for each configuration of the parameters, 500,000 photons are collected. Because the black hole (BH) absorption and the collision between the photons and the accretion disk (we ignore the disk reflection), the seed photon number $N_{seed} \geq 500,000$. In each simulation, six spectra will be produced by collecting the output photons in different directions from 0^0 to 35^0 , 35^0 to 45^0 , 45^0 to 55^0 , 55^0 to 65^0 , 65^0 to 75^0 , 75^0 to 85^0 degrees, corresponding to the inclination angles $22.7, 40.1, 49.9, 59.8, 69.6, 79.2$ degrees respectively (by considering the solid angle and disk projection). To make a connection between the seed photon number in our simulation and the real disk flux, each spectrum had been scaled down by a factor f_{scale} , which is determined by,

$$f_{scale} = N_{seed}/ph \quad (\text{A3})$$

To get the spectrum observed at different inclination angles, each angle-dependent spectrum has been scaled down by different area factors Δs_θ to get the average flux at that inclination angle, which is determined by,

$$\begin{aligned} \Delta s_\theta &= \int_{\theta_i}^{\theta_j} D^2 \sin(\theta) d\theta \int_0^{2\pi} d\phi \\ &= 2\pi D^2 [\cos(\theta_i) - \cos(\theta_j)] \end{aligned} \quad (\text{A4})$$

If we take $r_{in} = 1$ km, $D = 10$ kpc in equation (A2) (in order to compare with *diskbb* in *XSPEC*), the relation between real r_{in} and normalization of the table model is,

$$K_{norm} = \left(\frac{r_{in}/km}{D/10kpc} \right)^2 \quad (\text{A5})$$

REFERENCES

Akhiezer, A. J. & Berestetski, V. B. 1965, Quantum Electrodynamics (New York: Interscience Publications).

Berestetski, V. B., Lifshitz, E. M., & Pitaevski, L. P. 1972, Relativistic Quantum Theory (Oxford, New York: Pergamon Press).

Boella, G., Chiappetti, L., Conti, G., Cusumano, G., del Sordo, S., La Rosa, G., Maccarone, M. C., Mineo, T., Molendi, S., Re, S., Sacco, B. & Tripiciano, M. 1997, A&AS, 122, 327

Campana, S., Stella, L., Belloni, T., Israel, G. L., Santangelo, A., Frontera, F., Orlandini, M. & Dal Fiume, D. 2002, A&A 384, 163

Corman, E. G. 1970, Phys. Rev., D1, 2734

Cunningham, C. T. 1975, ApJ, 202, 788

Fenimore, E. E., Klebesadel, R. W., Laros, J. G., Stockdale, R. E. & Kane, S. R. 1982, Nature, 297, 665

Frontera, F., Costa, E., dal Fiume, D., Feroci, M., Nicastro, L., Orlandini, M., Palazzi, E. & Zavattini, G. 1997, A&AS, 122, 357

Gierliński, M., Zdziarski A. A., Poutanen J., Coppi P. S., Ebisawa K., & Johnson W. N., 1999, MNRAS, 309, 496

Gierliński, M., Maciołek-Niedźwiecki, A., and Ebisawa, K. 2001, MNRAS, 325, 1253

Gorécki, A. & Wilczewski, W. 1984, Acta Astron., 34, 141

Haardt F. & Maraschi, L. 1991, ApJ380, L51

Hua, X.-M. 1997, Computers in Physics, Vol. 11, No. 6

Hua, X.-M. & Titarchuk, L. 1995, ApJ, 449, 188

Klein, O. & Nishina, Y. 1929, *Zs. f. Phys.*, 52, 853

Kubota, A., Makishima, K. & Ebisawa, K. 2001, ApJ, 560, L147

Lewin, W. H., Van Paradijs, J. & van den Heuvel, E. P. J. 1995, X-Ray Binaries, Cambridge University Press, ISBN 0-521-59934-2

Loh, E. D. & Garmire, G. P. 1971, ApJ166, 301

Longair, M. S. 1992, High Energy Astrophysics (2nd edition), vol 1, P98

Makishima, K., Maejima, Y., Mitsuda, K., Bradt, H. V., Remillard, R. A., Tuohy, I. R., Hoshi, R. & Nakagawa, M. 1986, ApJ 308, 635

Manzo, G., Giarrusso, S., Santangelo, A., Ciralli, F., Fazio, G., Piraino, S. & Segreto, A. 1997, A&AS, 122, 341

Mitsuda, K., Inoue, H., Koyama, K., Makishima, K., Matsuoka, M., Ogawara, Y., Suzuki, K., Tanaka, Y., Shibasaki, N. & Hirano, T. 1984, PASJ, 36, 741

Nayakshin, S. & Dove, J. B. 2001, ApJ, 560, 885

Parmar, A. N., Martin, D. D. E., Baudaz, M., Favata, F., Kuulkers, E., Vacanti, G., Lammer, U., Peacock, A. & Taylor, B. G. 1997, A&AS, 122, 309

Payne, D. G. 1980, ApJ, 237, 951

Poutanen, J. & Svensson, R. 1996, ApJ, 470, 249

Pozdnyakov, L. A., Sobol, J. M. & Sunyaev, R. A. 1977, Sov. Astron.-AJ, 21 708

Remillard, R., Levine, A., Wood, A., Wagner, R. M., Starrfield, S., Shrader, C., Bowell, E., Skiff, B. & Koehn, B. 1998, IAUC 6920

Rybichi, G. B. & Lightman, A. P. 1979, Radiative Processes in Astrophysics, A Wiley-Interscience Publication, ISBN 0471-04815-1, P207

Shakura, N. I. & Sunyaev, R. A. 1973, A&A, 24, 337

Shimura, T & Takahara, F. 1995, ApJ, 445, 780

Skibo, J., Dermer, C. D., Ramaty, R. & McKinley, J. M. 1995, ApJ, 446, 86

Sobczak, G. J., McClintock, J. E., Remillard, R. A., Levine, Alan M., Morgan, E. H., Bailyn, C. D. & Orosz, J. A. 1999a, ApJ, 517, L121

Sobczak, G. J., McClintock, J.E., Remillard, R. A., Bailyn, C. D. & Orosz, J. A. 1999b, ApJ, 520, 776

Sobol', J. M. 1974, The Monte-Carlo Methods (The University of Chicago Press).

Stern, B. E., Poutanen, J., Svensson, R., Sikora, M. & Begelman, M. C. 1995, ApJ, 449, L13

Sunyaev, R. A. & Titarchuk, L. G. 1980, A&A, 86, 121

Tanaka, Y. & Lewin, W. 1995, in X-ray Binaries, eds. W.H.G. Lewin, J. van Paradijs, & E.P.J. van den Heuvel, Cambridge U. Press, Cambridge) 126

Titarchuk, L. 1994, ApJ, 434, 570

Titarchuk, L. & Lyubarskij, Y 1995, *ApJ*, 450, 876

Wang, D., Yao, Y., Fukui W., Zhang, S. N., & Williams, R. 2004, *ApJ*, submitted

White, N. E., Ueda, Y., Dotani, T. & Nagase, F. 1998, *IAUC* 6927

Yao, Y., Wang, Q. D., Zhang, S. N., Zhang, X., & Fukui, W. 2004, *ApJ*, in preparation

Zhang, S. N., Cui, W & Chen, W. 1997, *ApJ*, 482L, 155Z

Zhang, S. N., Cui, W., Chen, W., Yao, Y., Zhang, X., Sun, X., Wu, X., & Xu, H. 2000, *Science*, 287, 1239

Zhang, X., Zhang, S. N., & Yao, Y. 2001, *AIP Conference Series*, 587, 101

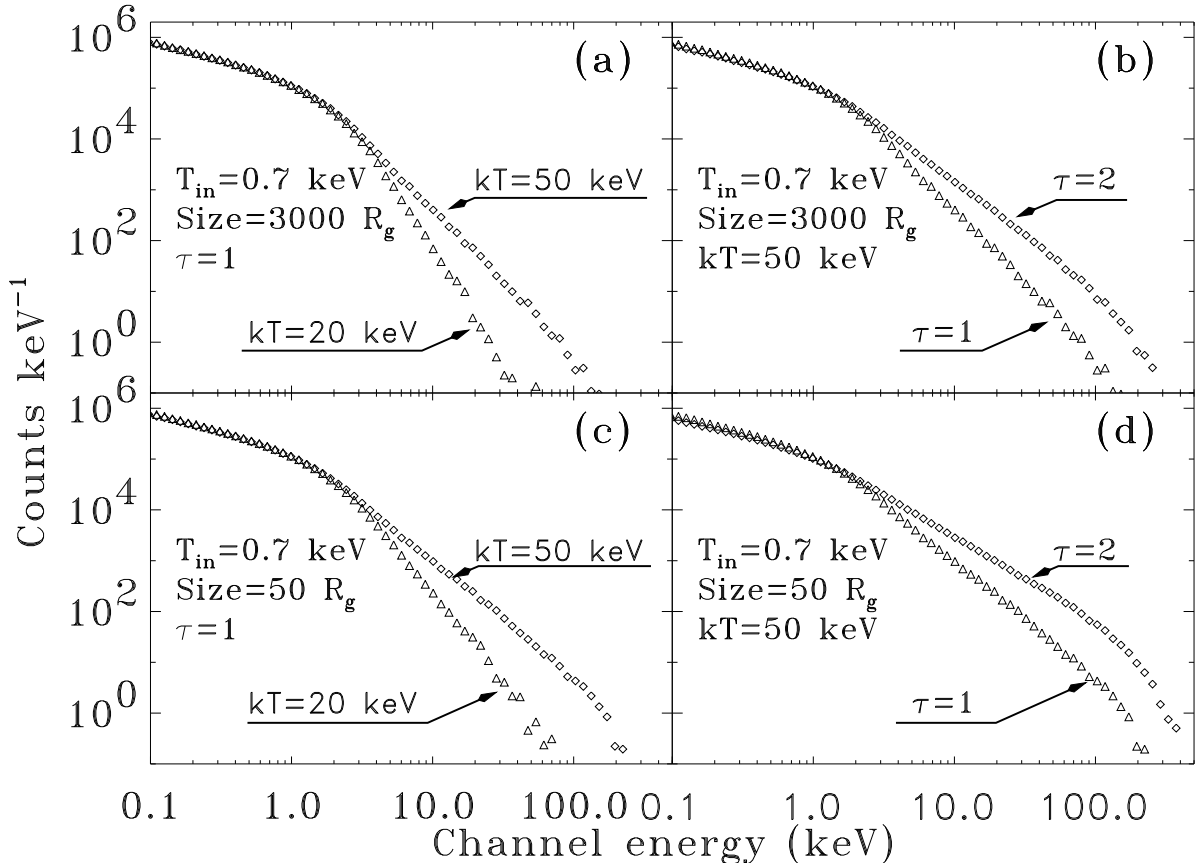


Fig. 1.— The high energy part of the output spectra is determined by the y -parameter if the electron energy distribution follows the thermal form in the corona. The input parameters of the system are indicated in the plots, where T_{in} is the inner disk temperature, kT is the corona temperature, $Size$ is the corona size and τ is the optical depth of the corona. Panel (a) shows how the electron temperature in the spherical corona affects the output spectrum. Panel (b) shows how the optical depth of the spherical corona affects the output spectra. Panels (c) and (d) are the same as Panels (a) and (b), but for systems with disk-like coronae.

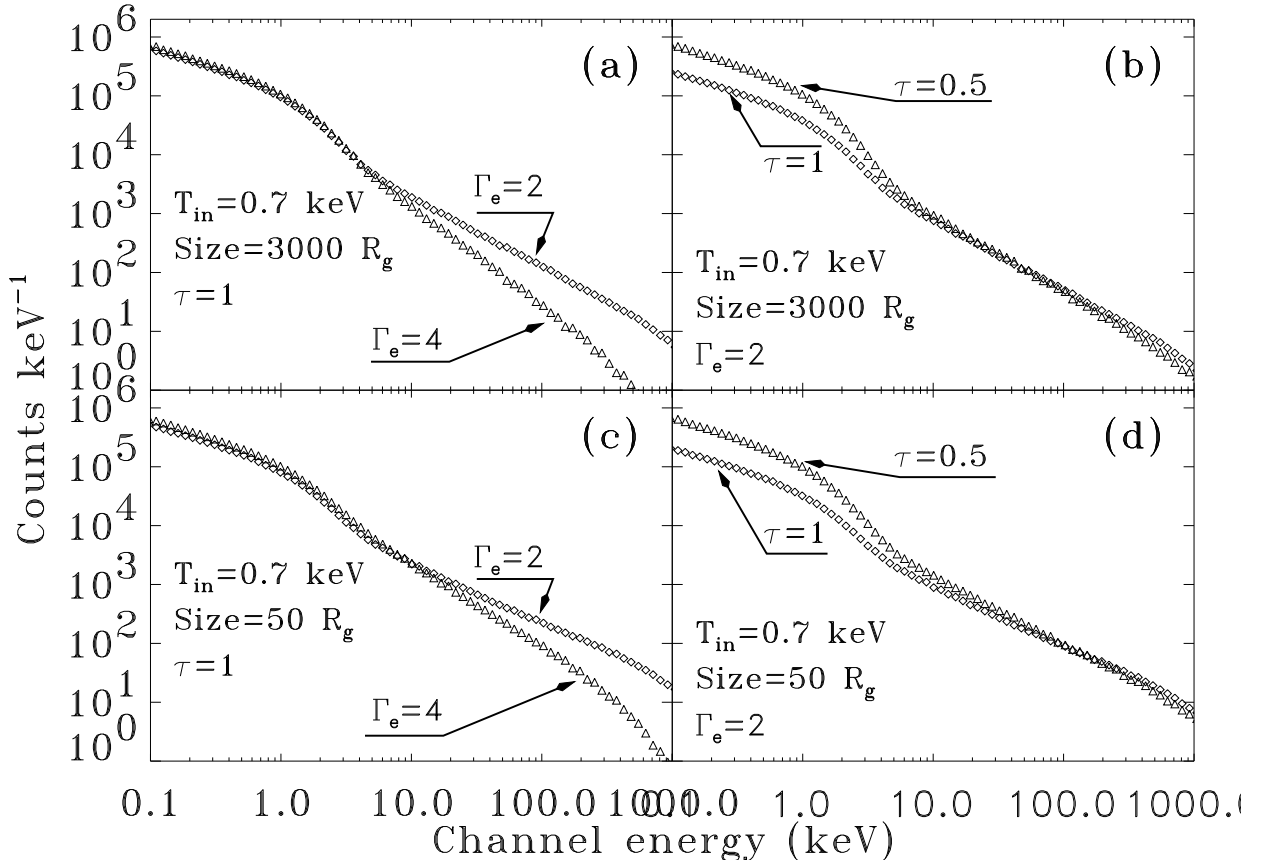


Fig. 2.— The spectra for the power-law electron distribution in the corona. Γ_e is the electron power-law index in the corona. Panel (a) shows in the spherical corona, how different electron indices affect the spectra and Panel (b) shows how the optical depth of the corona affect the spectra. Panels (c) and (d) illustrate the same comparisons as Panels (a) and (b), but for systems with disk-like coronae.

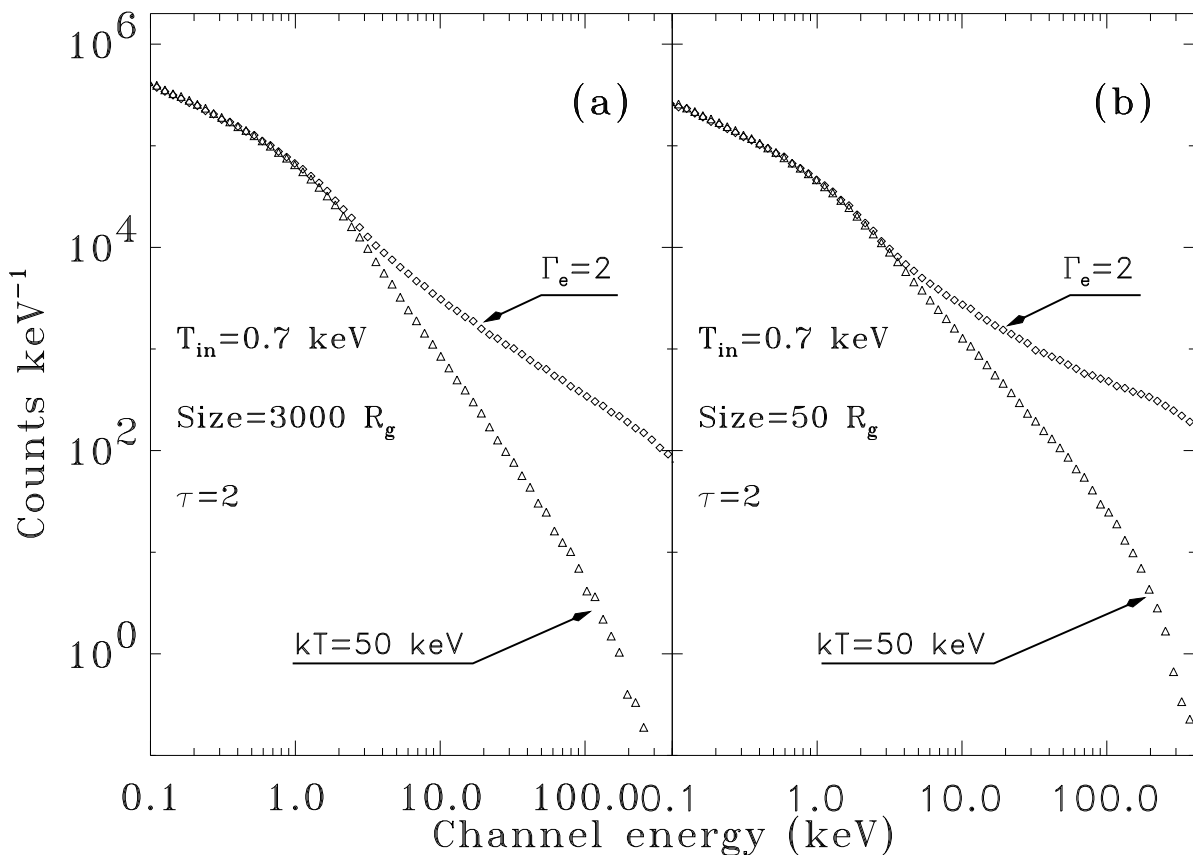


Fig. 3.— Panel (a) shows that in a spherical corona, the hard tails of the output spectra are different when electron energy distribution in the corona follows a power-law form (indicated by Γ_e) or follows a thermal form (indicated by kT). Panel (b) shows the same comparison but for a disk-like corona.

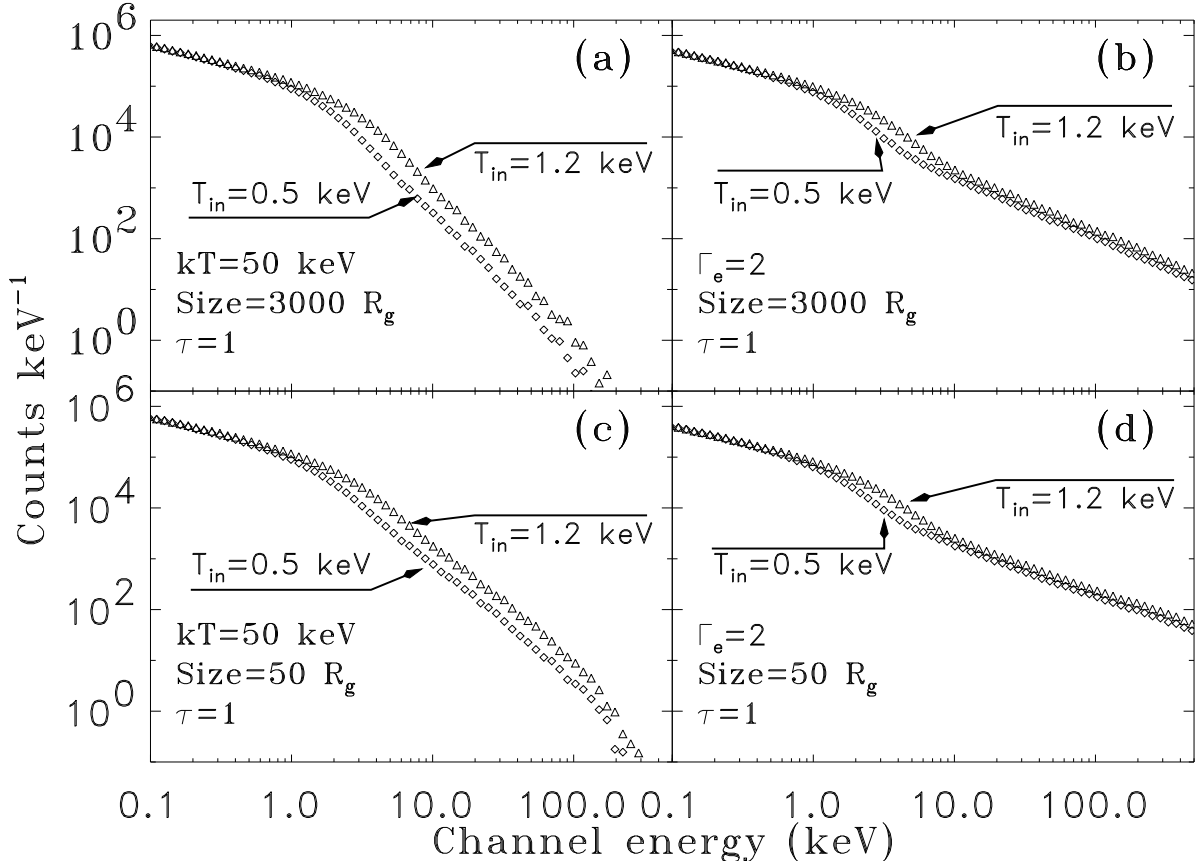


Fig. 4.— The turning point in the soft band of the spectrum is determined by the inner disk temperature. Panels (a) and (b) show how the inner disk temperature affect the spectra for the system with thermal electrons (Panel a) and power-law electrons (Panel b) in the spherical corona. Panels (c) and (d) shows the same comparison, but for systems with disk-like corona.

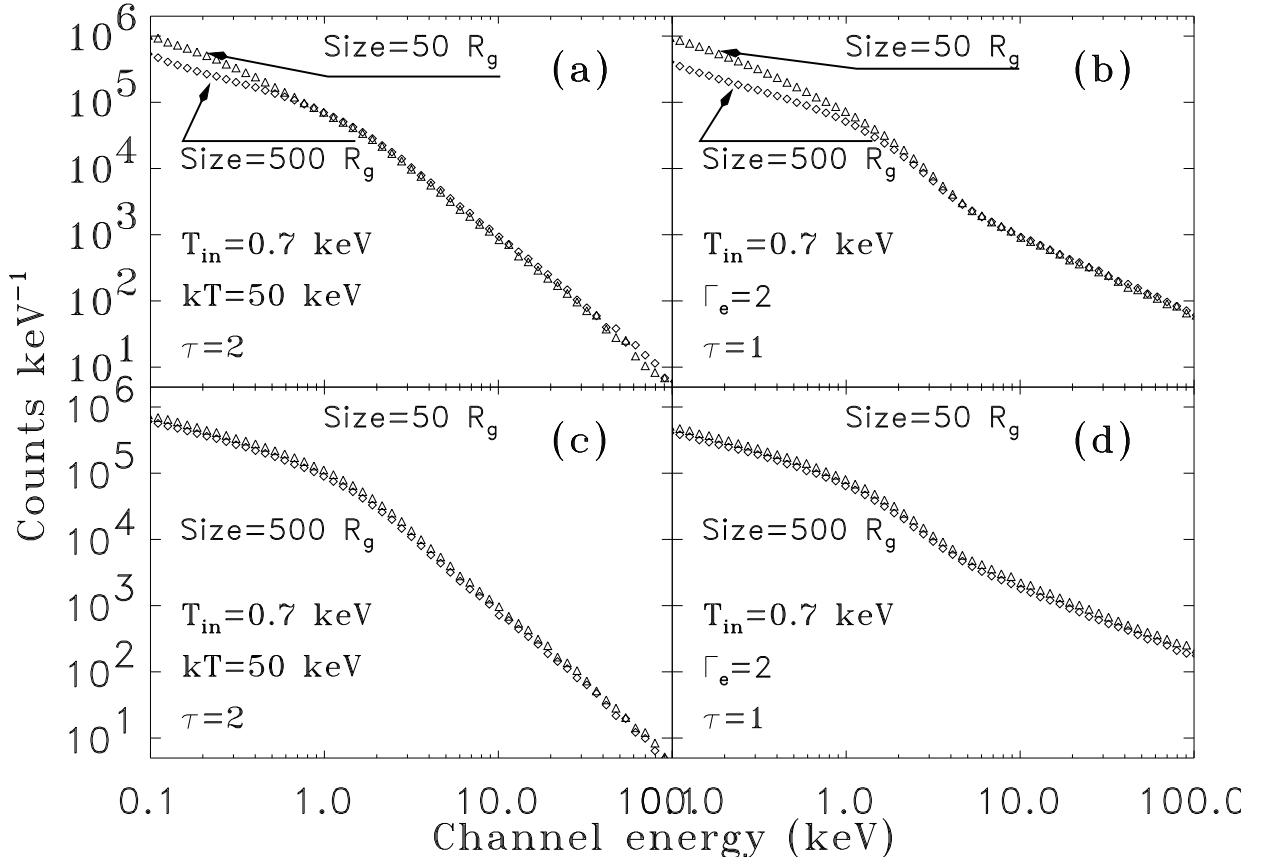


Fig. 5.— The spectrum in the low energy band is related to the size of the spherical corona, but is not related to the size of the disk-like corona. Panel (a) shows the differences of the spectra for the system with thermal electrons with different sizes of a spherical corona, whereas Panel (b) shows the differences of the spectra for the system with power-law electrons with different sizes of a spherical corona. Panels (c) and (d) show the same comparison as Panels (a) and (b), but for the system with the disk-like corona.

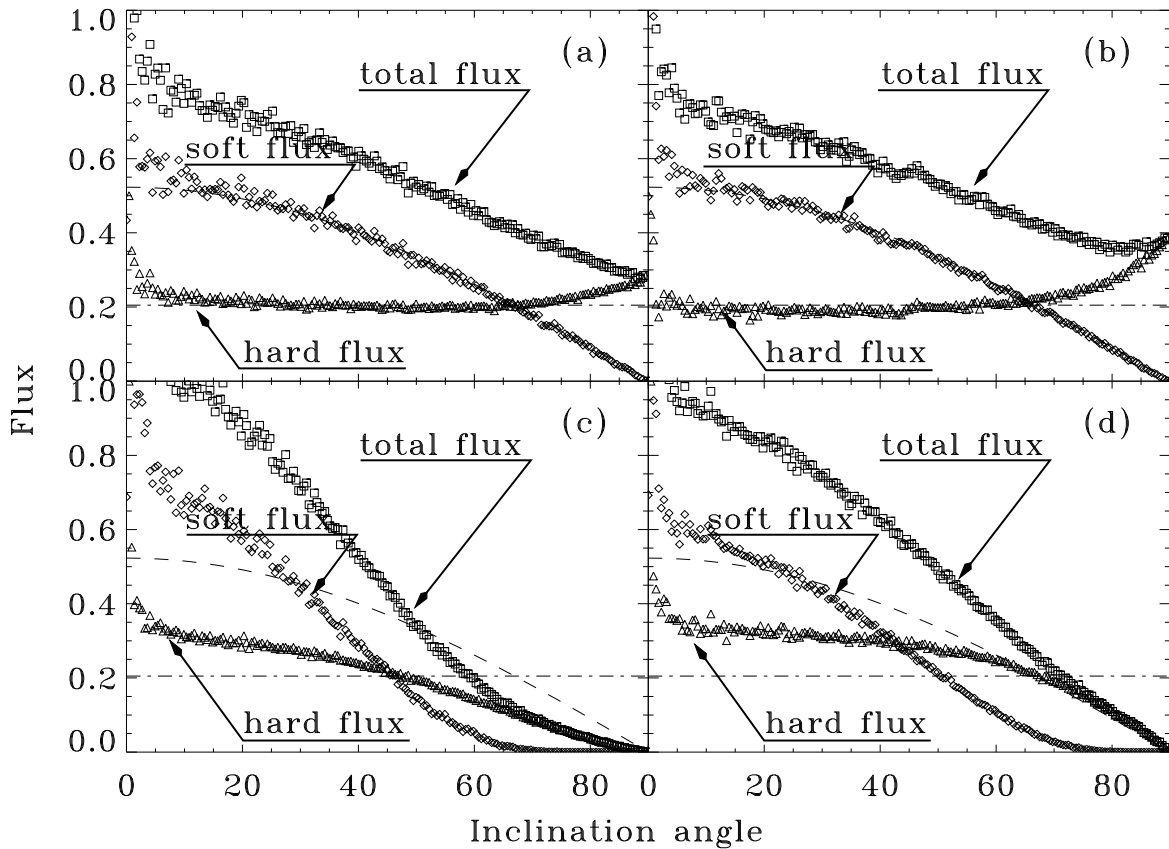


Fig. 6.— The angular dependency of the flux. Panel (a) shows the angular distribution of the flux of different spectral components for the system with thermal electrons in the spherical corona. Panel (b) shows the angular distribution of the flux for the system with power-law electrons in the spherical corona. Panel (c) and (d) show the same comparisons but for the system with the disk-like corona.

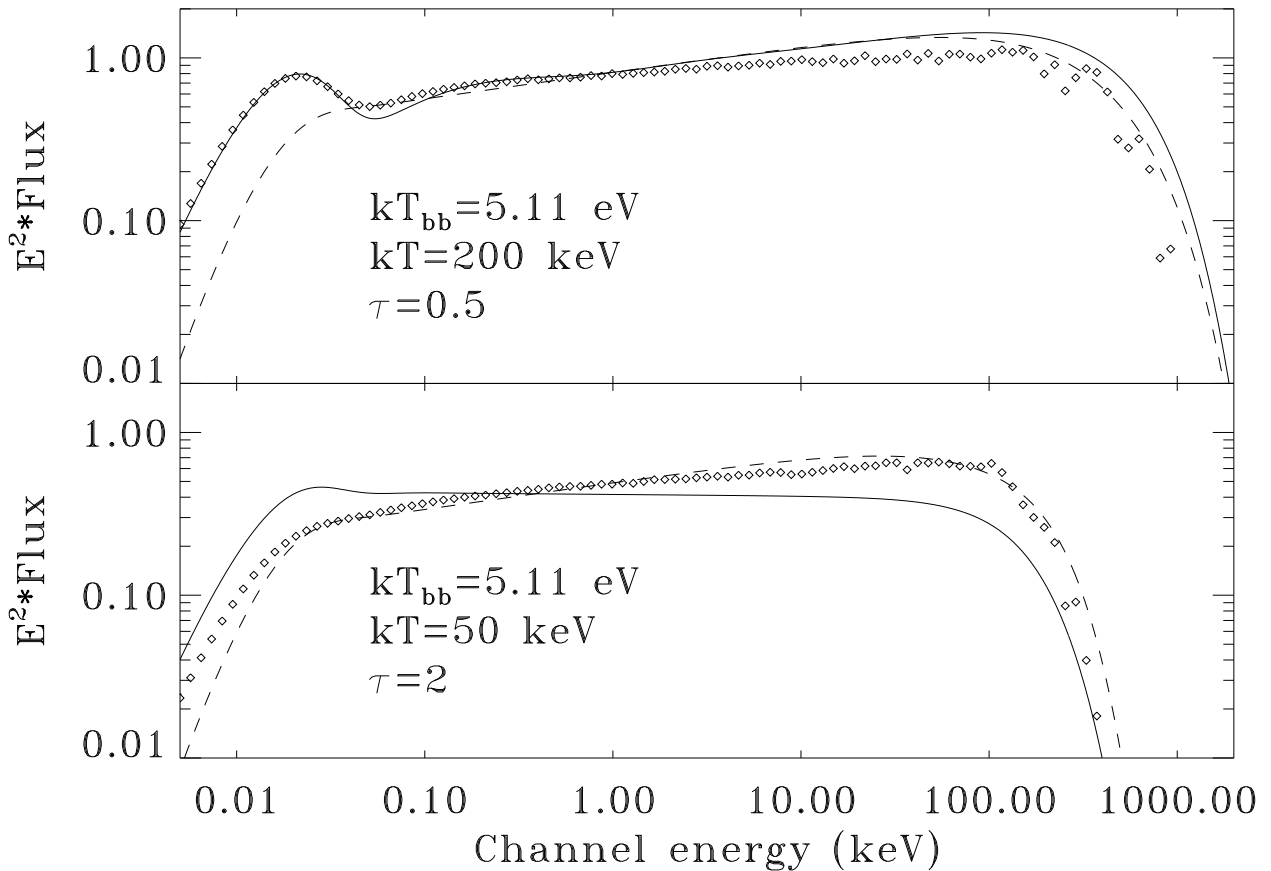


Fig. 7.— Angle-averaged Comptonized spectra E^2*Flux from a spherical corona as a function of photon energy. The incident photons are assumed from the center of the corona. The *diamond symbols*: results from our simulation; *solid line*: results from Poutanen & Svensson (1996, PS96); *dashed line*: results from Titarchuk (1994, T94). In PS96 and our simulation, blackbody incident photons are used, and in T94 Wien incident photons with the same temperature kT_{bb} as the blackbody are used. The kT is the electron thermal temperature in the corona and τ is the Thomson optical depth of the corona.

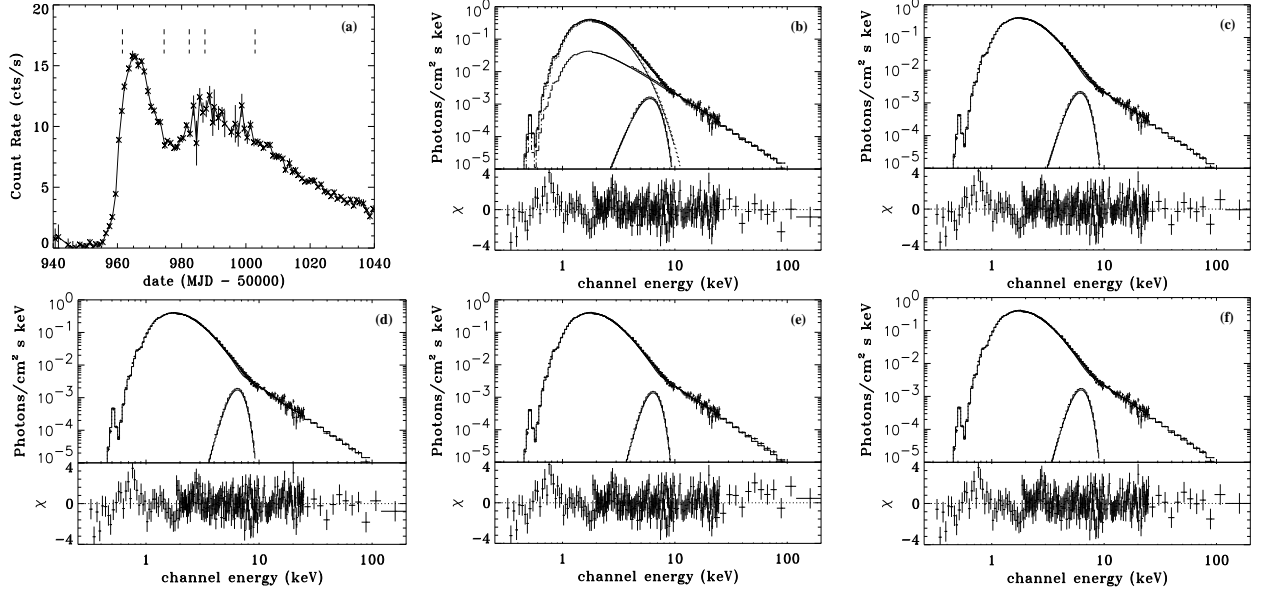


Fig. 8.— Panel (a) is the ASM/RXTE light curve of the black hole candidate XTE J2012+381 during its outburst in 1998; the dotted lines indicate the dates of BeppoSAX observations we have analyzed. The first observation is in the rising phase in which the hard component is relatively strong whereas the other four observations are in the soft state. Panel (b) shows the unfolded spectrum and the residuals for the first observation modeling with *diskbb + powerlaw* with inter-stellar absorption and a Gaussian line. The best fit parameters are: $n_H = 1.36 \pm 0.02 \times 10^{22} \text{ cm}^{-2}$, $T_{in} = 0.75 \pm 0.01 \text{ keV}$, $K_{BB} = 1097 \pm 50$, $\Gamma = 2.22 \pm 0.04$, $norm = 0.32 \pm 0.05$, $E_{gauss} = 6.1 \pm 0.2 \text{ keV}$, $\sigma_{gauss} = 1.0 \pm 0.2 \text{ keV}$, $norm_{gauss} = (3.5 \pm 0.4) \times 10^{-3}$, and the Chi-Squared is 277 with 244 degrees of freedom. Panels (c), (d), (e), (f) are unfolded spectra and the residuals for the first observation modeling with our table models, where (c) and (d) are for the powerlaw electron energy distribution in a spherical corona and in a disk-like corona respectively, and (e) and (f) are for the thermal electron energy distribution in a spherical and in a disk-like corona respectively. The best fit parameters are listed in Table 1.

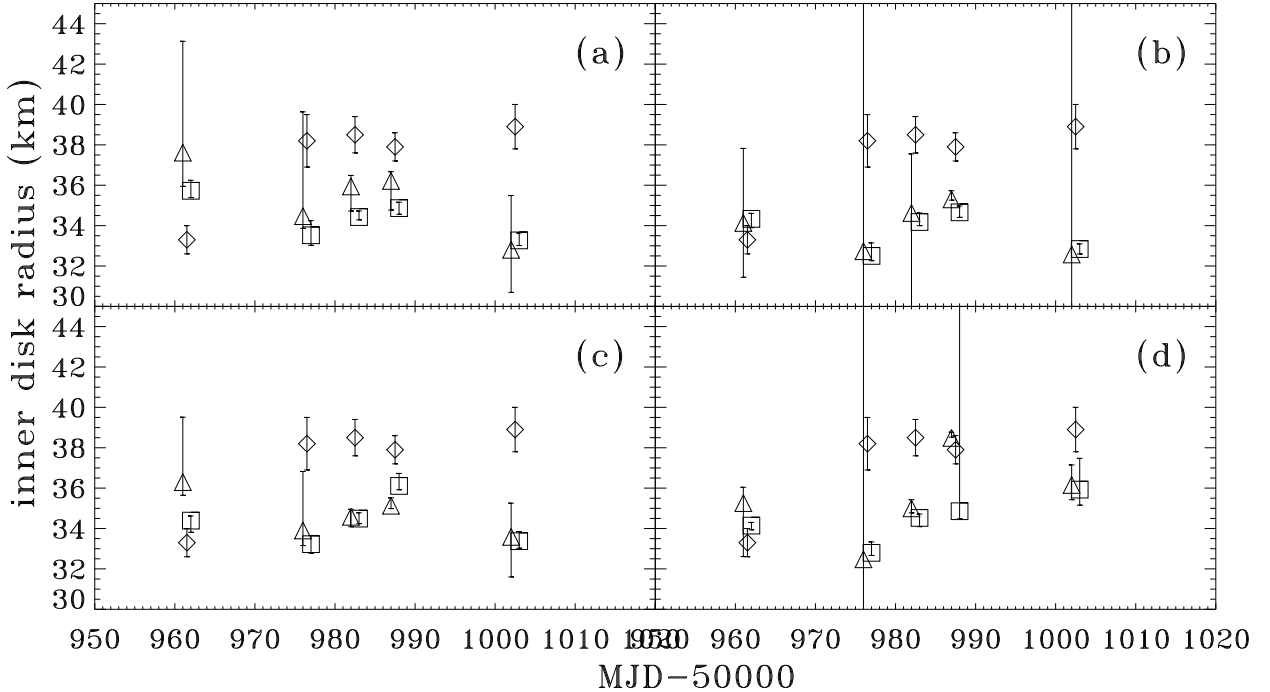


Fig. 9.— The inner radius of the accretion disk inferred from our table models for different configurations of the system (listed in the plot) and those by Campana (2002, inferred from model-fit with *diskbb + powerlaw*). In order to show the comparison clearly, we shift the observation date slightly in the plot. The results indicated by rectangles are inferred from the same table model as those indicated by the triangles, except that the Hydrogen density is fixed to $1.33 \times 10^{22} \text{ cm}^{-2}$ and inclination angle is fixed at 40 degrees.

Table 1: The fitting results with table models. Model-A is the table model with powerlaw electron energy distribution in the spherical corona. Model-B is the table model with powerlaw electron energy distribution in the disk-like corona. Model-C is the table model with thermal electron energy distribution in the spherical corona and model-D is the table model with thermal electron energy distribution in the disk-like corona.

model – A									
obsid (MJD)	N_H (10^{22} cm^{-2})	T_{in} (keV)	Γ_e	Size (R_g)	τ	θ ($^{\circ}$)	K^a $norm$ (km^2)	χ^2 (/dof)	K'^b $norm$ (km^2)
50961	$1.35^{+0.01}_{-0.03}$	$0.720^{+0.002}_{-0.002}$	$4.2^{+0.1}_{-0.3}$	82^{+22}_{-34}	$0.245^{+0.073}_{-0.058}$	27^{+34}_{-34}	1589^{+139}_{-500}	276(/242)	1666^{+49}_{-43}
50976	$1.31^{+0.02}_{-0.02}$	$0.706^{+0.003}_{-0.003}$	$4.5^{+0.7}_{-0.5}$	61^{+39}_{-93}	$0.103^{+0.022}_{-0.017}$	24^{+35}_{-35}	1260^{+406}_{-406}	199(/170)	1467^{+64}_{-55}
50982	$1.35^{+0.04}_{-0.04}$	$0.714^{+0.002}_{-0.002}$	$5.0^{+1.0}_{-0.5}$	84^{+64}_{-64}	$0.095^{+0.016}_{-0.006}$	$24(fix)$	1370^{+91}_{-42}	185(/195)	1547^{+12}_{-27}
50987	$1.34^{+0.01}_{-0.02}$	$0.726^{+0.001}_{-0.004}$	$6.0^{+**}_{-0.1}$	11^{+1}_{-1}	$0.070^{+0.008}_{-0.006}$	26^{+**}_{-13}	1463^{+114}_{-37}	196(/147)	1587^{+28}_{-27}
51002	$1.32^{+0.02}_{-0.02}$	$0.707^{+0.002}_{-0.002}$	$6.0^{+0.2}_{-0.2}$	15^{+3}_{-14}	$0.071^{+0.009}_{-0.009}$	40^{+**}_{-12}	1407^{+175}_{-240}	157(/148)	1445^{+31}_{-32}
model – B									
50961	$1.34^{+0.01}_{-0.02}$	$0.724^{+0.003}_{-0.004}$	$4.0^{+0.1}_{-0.1}$	–	$0.072^{+0.017}_{-0.011}$	60^{+7}_{-5}	2286^{+346}_{-521}	274(/242)	1539^{+39}_{-25}
50976	$1.31^{+0.02}_{-0.02}$	$0.707^{+0.003}_{-0.004}$	$4.8^{+0.8}_{-0.4}$	–	$0.021^{+0.007}_{-0.014}$	69^{+10}_{-10}	3031^{+1825}_{-599}	203(/171)	1379^{+20}_{-55}
50982	$1.32^{+0.03}_{-0.01}$	$0.711^{+0.003}_{-0.002}$	$5.7^{+0.3}_{-0.3}$	–	$0.022^{+0.012}_{-0.010}$	69^{+9}_{-10}	3401^{+1381}_{-599}	182(/196)	1525^{+40}_{-22}
50987	$1.33^{+0.01}_{-0.01}$	$0.724^{+0.001}_{-0.002}$	$5.5^{+0.3}_{-0.3}$	–	$0.006^{+0.001}_{-0.001}$	63^{+1}_{-2}	2778^{+68}_{-6}	189(/148)	1568^{+29}_{-21}
51002	$1.31^{+0.02}_{-0.02}$	$0.706^{+0.001}_{-0.002}$	$5.6^{+**}_{-0.3}$	–	$0.012^{+0.002}_{-0.004}$	57^{+**}_{-12}	1949^{+789}_{-4031}	156(/149)	1408^{+22}_{-22}
model – C									
obsid (MJD)	N_H (10^{22} cm^{-2})	T_{in} (keV)	kT^g (keV)	Size (R_g)	τ	θ ($^{\circ}$)	K_{norm} (km^2)	χ^2 (/dof)	K'^b $norm$ (km^2)
50961	$1.37^{+0.01}_{-0.02}$	$0.729^{+0.001}_{-0.003}$	$200.0^{+9.3}_{-9.3}$	20^{+4}_{-4}	$0.237^{+0.027}_{-0.006}$	23^{+24}_{-24}	1383^{+49}_{-255}	292(/242)	1544^{+51}_{-21}
50976	$1.33^{+0.03}_{-0.03}$	$0.707^{+0.004}_{-0.005}$	$200.0^{+38.0}_{-38.0}$	10^{+**}_{-16}	$0.111^{+0.111}_{-0.016}$	23^{+**}_{-40}	1202^{+53}_{-217}	207(/170)	1441^{+38}_{-38}
50982	$1.33^{+0.03}_{-0.02}$	$0.713^{+0.003}_{-0.004}$	$99.6^{+19.6}_{-19.6}$	49^{+18}_{-18}	$0.070^{+0.006}_{-0.004}$	59^{+5}_{-8}	2357^{+65}_{-50}	179(/195)	1553^{+26}_{-22}
50987	$1.33^{+0.03}_{-0.03}$	$0.730^{+0.006}_{-0.002}$	$5.8^{+0.8}_{-0.8}$	99^{+10}_{-10}	$0.098^{+0.019}_{-0.019}$	$59(fix)$	2432^{+54}_{-54}	197(/148)	1702^{+59}_{-59}
51002	$1.31^{+0.01}_{-0.01}$	$0.709^{+0.003}_{-0.003}$	$5.5^{+1.0}_{-0.5}$	99^{+20}_{-20}	$0.097^{+0.017}_{-0.017}$	29^{+**}_{-46}	1293^{+148}_{-132}	175(/149)	1454^{+42}_{-42}
model – D									
50961	$1.35^{+0.02}_{-0.02}$	$0.722^{+0.003}_{-0.003}$	$158.4^{+12.3}_{-13.2}$	–	$0.116^{+0.007}_{-0.009}$	23^{+**}_{-5}	1300^{+30}_{-58}	280(/243)	1522^{+19}_{-14}
50976	$1.31^{+0.03}_{-0.03}$	$0.708^{+0.003}_{-0.002}$	$200.0^{+40.0}_{-40.0}$	–	$0.015^{+0.017}_{-0.017}$	61^{+8}_{-8}	2172^{+1060}_{-1060}	208(/171)	1404^{+47}_{-47}
50982	$1.33^{+0.02}_{-0.02}$	$0.713^{+0.002}_{-0.001}$	$99.8^{+8.7}_{-13.2}$	–	$0.050^{+0.005}_{-0.007}$	23^{+**}_{-5}	1281^{+17}_{-31}	179(/196)	1556^{+39}_{-17}
50987	$1.34^{+0.01}_{-0.01}$	$0.720^{+0.001}_{-0.002}$	$10.5^{+1.2}_{-0.5}$	–	$0.222^{+0.013}_{-0.021}$	$23(fix)$	1549^{+3}_{-23}	193(/149)	1586^{+34}_{-34}
51002	$1.32^{+0.02}_{-0.01}$	$0.701^{+0.004}_{-0.001}$	$13.0^{+1.5}_{-0.7}$	–	$0.281^{+0.061}_{-0.085}$	$23(fix)$	1367^{+55}_{-76}	166(/150)	1685^{+18}_{-72}

^{**}the limit is not reachable.

^aNormalization of the table model, $K_{norm} = ((R_{in}/\text{km})/(D/10\text{kpc}))^2$.

^bNormalization of the table model as a , but inferred by fixing the Hydrogen density and the inclination angle. Please see text for detail.